HHS Public Access

Author manuscript

Magn Reson Med. Author manuscript; available in PMC 2018 August 01.

Published in final edited form as:

Magn Reson Med. 2017 August ; 78(2): 689–701. doi:10.1002/mrm.26387.

Volumetric Quantification of Absolute Local Normalized Helicity in Patients with Bicuspid Aortic Valve and Aortic Dilatation

Julio Garcia, PhD[1,2], **Alex J Barker, PhD**[1], **Jeremy D Collins, MD**[1], **James C Carr, MD**[1], and **Michael Markl, PhD**[1,3]

[1] Department of Radiology, Northwestern University, Chicago, USA.

[2] Department of Cardiac Sciences – Stephenson Cardiac Imaging Centre, Cumming School of Medicine, University of Calgary, Calgary, AB, Canada.

[3] Biomedical Engineering, Northwestern University, Evanston, USA.

Abstract

Purpose—Absolute local normalized helicity (LNH) can differentiate flow alterations in the aorta between healthy controls and bicuspid aortic valve (BAV) patients.

Methods—65 controls and 50 subjects with BAV underwent in-vivo 4D flow MRI. Data analysis included the 3D segmentation of the thoracic aorta (ascending aorta, aortic arch and descending aorta) and calculation of absolute LNH. The mean velocity in the entire aorta was used to identify peak systole, systolic deceleration and mid-diastole. A sensitivity analysis was performed to identify the optimal absolute LNH threshold comparing control and BAV groups. A reproducibility test was performed for 3D segmentation and absolute LNH.

Results—Absolute LNH above 0.6 was significantly higher ($P<0.001$) in BAV in comparison to controls for all aortic segments and cardiac time frames. Absolute LNH in the ascending aorta correlated with maximal aortic diameter ($r=0.83$, $P<0.001$, at peak systole; $r=0.84$, $P<0.001$, at systolic deceleration; $r=0.88$, $P<0.001$, at mid-diastole) and significantly increased ($P<0.001$) with aortic stenosis severity. Intra- and inter-observer errors were 5±2% and 12±6% for 3D segmentation and 7±6% and 12±7% for absolute LNH.

Conclusion—Absolute LNH can differentiate between controls and subjects with aortic dilatation, and was associated with maximal aortic diameter and aortic stenosis severity.

Keywords

aortic diseases; flow helicity; hemodynamics

Corresponding author: Julio Garcia, Ph.D., Department of Cardiac Sciences – Stephenson Cardiac Imaging Centre, University of Calgary – Cumming School of Medicine, 1403 – 29th Street NW, Suite 0700-SSB, Calgary, AB, CANADA, T2N 2T9, Phone: (403) 944-1211, julio.garciaflores@ucalgary.ca.

Disclosures

The authors declare that they have no competing interests.

INTRODUCTION

The curved non-planar geometry of the human thoracic aorta leads blood ejected from the heart to develop helical flow patterns (1). Helical flow, corkscrew-like motion about the principal flow direction, has been reported as a normal observation in healthy subjects (2–4). Helical flow in the thoracic aorta may be exacerbated by common pathologies such as aortic dilatation, aortic valve stenosis, or bicuspid aortic valve (BAV) (5–9). In turn, increased helical flow can influence the distribution of shear forces at the vessel wall and contribute to the changes in endothelial cell function thereby promoting arterial remodeling (5,7,10,11). Helical flow can be evaluated invivo using four dimensional (4D) flow MRI which facilitates the acquisition of time-resolved 3-dimensional flow velocities with full volumetric coverage of the entire thoracic aorta (7,12,13). Previous studies have qualitatively estimated helical flow through 3D flow visualization and assessment of pathlines, streamlines, or flow vectors (14–17). These approaches to analysis and classify helical flow could remain observer dependent. A more quantitative approach to assess flow helicity can be achieved by parameters such as vorticity magnitude threshold, Q-criterion, λ_2-criterion, and local normalized helicity (LNH) (13,18–20).

In particular, LNH measures the local alignment between the velocity and the vorticity vector fields, provides information about the organization of both laminar and turbulent flow, and is associated with flow energy decay over time (21,22). LNH has been explored using 2D velocity measurements, multi-planar reformatting of 4D flow MRI data and volumetric topologic visualization (13,23–26). In addition, some studies have shown that 4D flow MRI derived LNH can be useful to better understand complex flow pattern evolution through the formation and dissipation of volumetric flow helicity (13,24,26). A visualization threshold of ±0.8 for LNH has been used in previous studies with small populations to detect elevated LNH regions (23,25,27). However, a full 3D quantification methodology, the definition of optimal analysis thresholds, and reproducibility test for assessing and detecting regions with elevated LNH in larger populations are missing. This might limit the diagnostic value of LNH for the characterization of aortic and valvular diseases. Specially, BAV patients are prone to increase helical flow which might promote aortic dilatation (5,7,28). Thus, the association between quantitative 3D LNH and patients with BAV should be evaluated for a better understanding of local alterations in aortic dimensions. Moreover, aortic valve fusion pattern and aortic stenosis severity might similarly increase helical flow formation in the ascending aorta (5,6,28,29).

This study aims to exploit the full volumetric coverage of 4D flow MRI to demonstrate that: 1) the optimal selection of absolute LNH threshold may improve the assessment of elevated helicity in healthy controls and BAV patients; 2) absolute LNH quantification can differentiate helical flow alterations in the aorta between healthy controls and BAV patients with aortic dilatation; 3) absolute LNH is associated with BAV aortic dimensions, peak velocity, and aortic valve effective orifice area; 4) absolute LNH increases with aortic valve stenosis severity in BAV patients.

METHODS

Study population

Data from 115 subjects (65 healthy controls [age=43±14 years, 25 females] and 50 BAV patients [age=49±14 years, 12 females]) was included for analysis. The BAV patients were enrolled via an IRB-approved retrospective chart review for those who underwent a standard-of-care MRI between February 2014 and August 2014 for surveillance of aorta size. Heathy control volunteers underwent 4D flow MRI based on an IRB-approved prospective protocol and informed consent was obtained from all those participants.

Magnetic resonance imaging

MR imaging was performed on 1.5T (total n=74, healthy controls n=33, BAV=41) and 3T (total n=41, healthy controls n=32, BAV=9) systems (Magnetom Espree, Avanto, Aera and Skyra, Siemens, Erlangen, Germany) with dedicated body surface coils (Espree and Avanto: 6 elements coil + 6-9 in patient table for a total of 12-15 elements; Aera and Skyra: 18 elements coil + 12-18 elements in patient table for a total of 30-36 elements). All subjects underwent a standard-of-care thoracic cardiovascular MRI exam including dynamic 2D cine steady state free precession (SSFP) imaging of the heart and the aortic valve. The aortic valve images were used to determine valve morphology as previously reported (30). 4D flow MRI was acquired in a sagittal oblique 3D volume covering the thoracic aorta with prospective ECG-gating and a respiratory navigator placed on the lung-liver interface (12). Conventional parallel imaging, GRAPPA (GeneRalized Autocalibrating Partially Parallel Acquisitions), with a factor of R=2 was used. Pulse sequence parameters were as follows: TE=2.3–2.84 ms, TR= 4.6–5.4 ms, FOV= 212–540 mm×132–326 mm, true spatial resolution = 1.66–2.81×1.66–2.81×2.20–3.50 mm^3, temporal resolution = 36.8–43.2 ms, flip angle = 15°. Velocity encoding was adjusted to minimize velocity aliasing (1.5-4.0 m/s) based on the cine SSFP 3-chamber view of in-plane 2D phase-contrast scout images. A summary including the spatial resolution and velocity encoding selection for the controls group and BAV aortic stenosis sub-groups is provided in Table 1. 4D flow MRI acquisition times varied from 8 to 15 min depending on heart rate and navigator gating efficiency.

Data analysis

All 4D flow MRI data (Fig. 1A) were corrected for eddy currents, Maxwell terms, and velocity aliasing using custom built software (31) programmed in Matlab (Mathworks, Natick, Ma, USA). A 3D phase contrast (PC) MR angiogram (MRA) was computed for each subject using the pre-processed 4D flow MRI data as given by $I_i^{PC\quad MRA}(\overrightarrow{r}) = I_i^{Mag}(\overrightarrow{r}) \sqrt{\sum_{j=x,y,x} v_{j,i}^2(\overrightarrow{r})}$, where I_i^{Mag} is the magnitude image, $\overrightarrow{r}$ is the spatial location within the 3D volume, v is the velocity encoded image with j representing the velocity encoding direction in image coordinates (x, y, z), and i is the measured time frame within the cardiac cycle (12). The 3D PC MRA data were used to manually obtain a 3D segmentation (Mimics, Materialise, Leuven, Belgium) of the aortic lumen (Fig. 1B) (32). Anatomic landmarks were defined using the 3D PC MRA segmentation and the 4D flow MRI magnitude images, and used to subdivide the aorta 3D segmentation into three segments (Fig. 1C): ascending aorta (from left ventricle outflow

tract to brachiocephalic trunk [BCT]), aortic arch (from BCT to left subclavian artery [LSA]) and descending aorta (from LSA to the end of the segmentation). The maximal aortic diameter was calculated using equidistant planes along the 3D segmentation centreline in the ascending aorta segment (33,34). The 4D flow MRI dataset was subsequently masked using the full aorta 3D segmentation. The time-resolved masked aorta velocity field was then used to calculate the velocity magnitude (i.e. $V_{mag}=\sqrt{V_x^2+V_y^2+V_z^2}$). Mean velocity over the entire volume along the cardiac cycle was used to identify peak systole, systolic deceleration (between peak systole and end systole) and mid-diastolic time frames (Fig. 1D and Fig. 2). A maximum intensity projection (MIP) of *Vmag* was calculated in an oblique sagittal plane and averaged over three cardiac time frames centered on peak systole (32). The peak velocity in the ascending was extracted from the calculated *Vmag* MIP. Peak velocity was used to grade aortic stenosis severity and ranged between none (<2.0 m/s), mild (2.0-2.9 m/s), moderate (3.0-3.9 m/s), and severe (>4.0 m/s) overall subjects as indicated in the aortic valve guidelines (35). Aortic valve regurgitation severity (regurgitant fraction) was measured using an analysis plane at the sino-tubular junction (35). Aortic valve effective orifice area was calculated using the jet shear layer detection method (18,36,37).

Helicity calculation

LNH was calculated along the cardiac cycle as $LNH=\frac{V\cdot\omega}{|V||\omega|}$, where $\boldsymbol{V}$ and $\boldsymbol{\omega}$ are the masked velocity and the vorticity vectors (13,21,26). The vorticity was derived from $\boldsymbol{V}$ as $\boldsymbol{\omega}$=curl ($\mathbf{V}$) using a fourth-order compact Richardson scheme (18,37–39). The LNH calculation results in values between −1 and 1 (left-handed and right-handed rotation respectively) corresponding to the local angle between the velocity and the vorticity vectors. High values (±1) reflect regions where the flow rotation is reaching elevated helicity, and zero is obtained when the flow is symmetric. To assess both rotational directions the absolute LNH was used for analysis. A sensitivity analysis was performed to define which threshold was most sensitive to differences in absolute LNH between BAV and control groups. Gallo et al. defined a poor characterization of LNH at ±0.4 (27). Thus a threshold test range from 0.4 to 0.95 of absolute LNH was set, at each threshold the isosurface volume (in mm^3) was obtained. Furthermore, inter- and intra-observer variability between segmentations and calculation of absolute LNH were evaluated in 10 healthy control cases. Absolute error between measured volumes and Bland-Altman analysis were reported for both segmentation volume and absolute LNH using the optimal threshold from the sensitivity analysis.

Statistical analyses

All continuous data are presented as mean ± standard deviation. A Shapiro-Wilk test was used to evaluate distribution normality for measured parameters before performing a statistical comparison. Sensitivity analysis consisted of a statistical assessment between BAV and control groups for each evaluated segmentation (i.e. full aorta, ascending aorta, aortic arch, and descending aorta). Absolute error of aortic segmentation and absolute LNH was calculated by absolute error $(\%)=\frac{|measurement\ \ 2-measurement\ \ 1|}{measurement\ \ 1}\times 100$. For intra-observer absolute error measurement 1 was used as reference. For inter-observer absolute error measurement 1 from observed 1 was used as reference and measurement 2 was provided by

observer 2. Bland-Altman analysis was perform for both segmentation volume and calculation of absolute LNH using the optimal threshold from the sensitivity analysis. An independent-sample *t*-test was conducted to evaluate the significant differences between groups at peak systole, systolic deceleration and mid-diastolic frames. To compare measured parameters between heathy controls and BAV group an independent-sample *t*-test (Gaussian distribution) or Mann-Whitney test (non-Gaussian Distribution) was performed. Associations between maximal aortic diameter, aortic peak velocity, aortic valve effective orifice area, and absolute LNH in the ascending aorta were assessed by 2-tailed Pearson's correlation. P-values < 0.01 were considered significant. Statistical analysis was performed with SPSS 17 (SPSS, Chicago, IL).

RESULTS

Patient characteristics

The demographics of the study groups are summarized in Table 2. Patients in BAV group were significantly older (P=0.017) and taller (P=0.002) than healthy controls. Maximal aortic diameter was significantly higher in BAV group as compared with healthy controls (40±5 mm vs. 33±4 mm, P<0.001). In the BAV group n=10 (20%) patients presented with a peak velocity > 4 m/s (severe aortic stenosis). Aortic regurgitation was detected in 11 (22%) of BAV patients of which 1 (2%) was severe.

Local normalized helicity quantification

Absolute LNH was successfully extracted for all subjects. Sensitivity analysis P-values determined that 0.6 was the optimal threshold detecting most differences between groups at given time frames (Fig. 3). Thus, the data within this optimal threshold was used for further analysis. Aortic segmentation intra- and inter observer error were 5±2 % (measurement difference=−2517 mm^3, limits of agreement: −14,373 mm^3 to 9,703 mm^3) and 12±6 % (measurement difference=3287 mm^3, limits of agreement: −28,486 mm^3 to 25,060 mm^3) respectively. Absolute LNH intra- and inter observer error were 7±6 % (measurement difference=99 mm^3, limits of agreement: −3,187 mm^3 to 3,385 mm^3) and 12±7 % (measurement difference=1250 mm^3, limits of agreement: −5,233 mm^3 to 7,732 mm^3) respectively. Representative examples for one healthy control and one BAV patient (Fig. 2) illustrate the characteristic differences in aortic absolute LNH. Normal flow in controls at peak systole resulted in small and well organized absolute LNH structures. It was observed that LNH structures increased during deceleration and diastole (Fig. 2A). In contrast, LNH structures observed in BAV subjects led to marked local LNH elevation which persisted during late systolic deceleration and into diastole (Fig. 2B), in particular in the aortic valve region. As well, increased LNH appeared during mid-diastole in the descending aorta. Absolute LNH was significantly higher (P<0.001) in BAV patients in comparison with controls for all evaluated segments and cardiac phases (Fig. 4).

Absolute local normalized helicity association with aortic dilatation and peak velocity

Figure 5 summarizes the independent associations between maximal ascending aortic diameter and peak velocity with absolute LNH. Strong and significant relationships were found between maximal aortic diameter with elevated LHN at systolic deceleration (R=0.84,

P<0.001) and mid-diastole (R=0.88, P<0.001). Independent group-wise correlation analysis (i.e. controls and BAV) between maximal aortic diameter and elevated LNH are presented in Table 3, scatter plot provided as supporting Figure S1. In both groups maximal aortic diameter was significantly associated with elevated LNH. The pattern was particularly apparent for controls at peak systole and mid-diastole (R=0.84, P<0.001), and for BAV at systole deceleration (R=0.8, P<0.001) and mid-diastole (R=0.81, P<0.001). Correlation analysis remained similar after adjusting the aortic diameter by age.

Impact of aortic valve stenosis

Aortic valve effective orifice area showed a significant inverse relationship with elevated LNH, as presented in Figure 5. In particular, the pattern was apparent during peak systole (R=−0.31, P<0.001) and mid-diastole (R=−0.34, P<0.001). BAV patients with mild to severe aortic valve stenosis presented higher absolute LNH volumes in comparison with controls for all evaluated segments and cardiac time frames (Fig. 6). The presence of severe aortic stenosis significantly contributed to the development of elevated helicity along cardiac cycle as compared with controls (P<0.001). A summary of group comparisons is presented in Table 4, descriptive statistics provided as supporting Table S1. BAV maximum aortic diameters for mild (n=12), moderate (n=7) and severe (n=10) AS groups were similar (40±5 mm, 39±5 mm, and 41±4 mm, respectively). The severe AS group showed higher absolute LNH volume in the ascending aorta as compared with mild AS and moderate AS at peak systole (20%, and 35%, respectively), systolic deceleration (13%, and 31%, respectively), and mid-diastole (12%, and 25%, respectively). However, no significant differences between AS groups were found.

DISCUSSION

This study showed that: 1) optimal selection of threshold improves the volumetric assessment of absolute LNH; 2) elevated absolute LNH can differentiate helical flow patterns between healthy subjects and BAV patients; 3) absolute LNH was more closely associated with BAV maximal aorta diameter than aortic peak velocity or aortic valve effective orifice area; 4) valve stenosis increases absolute LNH in the ascending aorta; 5) absolute LNH demonstrated good reproducibility. The main contribution of this work was to introduce a novel quantitative volumetric method to assess complex flow patterns in the thoracic aorta and establish an optimal threshold for the assessment of aortic and valvular diseases. The systematic pre-processing and automatic calculation of absolute LNH demonstrated to have a good inter- and intra- reproducibility. Our findings showed that the aortic sub-volume exhibiting elevated absolute LNH was able to provide new quantitative information of aortopathy severity. The side-by-side visualization of the velocity magnitude MIPs and absolute LNH may be useful to easily identify regions where elevated helical flow occurs along the cardiac cycle.

Current clinical approach for adult BAV patients

State-of-the-art cardiac imaging is used for the diagnosis, phenotyping, and hemodynamic assessment of aortic valve dysfunction and the initial assessment of the thoracic aorta morphometry (40,41). In particular, close surveillance is recommended to detect changes in

aortic size, which may be triggered by coexisting mechanical, biological, and genetic influences (42). 4D flow MRI offers the opportunity to interrogate the velocities within the full volume of the thoracic aorta. The information from the aorta can be used to assess functional hemodynamic properties, blood flow patterns and advanced flow biomarkers (e.g. shear stress, strain, distensibility, complex helical flow). In this study a quantitative volumetric approach assessing complex flow patterns was applied using 4D flow-derived absolute LNH in order to complement the visualizations of the velocity field.

Helical flow quantification

The formation and dissipation of helical flow characterizes the local changes of blood flow structure over time (43). Therefore, helicity, like energy, has a great influence on the evolution and stability of both laminar and turbulent flows (21). In this study, we focused on helicity quantification using the absolute LNH. The presence of helical flow in the thoracic aorta is based on the assumption that valve morphology and aorta curved geometry may promote its formation. We showed, in Figure 2, that elevated helicity can be observed in healthy subjects and its formation is larger in BAV subjects with aortic dilatation. Helical flow patterns may play an important role by regulating the dissipation of energy and limiting flow instabilities (44,45). Previous studies (2,14) have shown that age-dependent changes in the thoracic aorta hemodynamics may be associated with an increase of the number of vortices (i.e. increase in helical flow). Furthermore, the effect of eccentric flow and the formation of helical patterns in BAV patients should be investigated in detail (7,28,29). In our study subjects were scanned using scanners at 1.5T and 3T. Strecker et al. demonstrated that 3T field strengths improves the 3D PC MRA, which was used for segmentation of the aorta, and not statically significant differences were found for systolic peak velocity (0.005 m/s, P=0.40) and net flow (3 mL/cycle, P=0.39) measurements as compared with 1.5T (46). A LNH threshold of ±0.8 has typically been used for visualization purposes to show the elevated helicity. To focus on the volumetric assessment of LNH the absolute value was used for simplicity. Note that this approach may omit potentially valuable information associated with flow rotation direction. In this study, we performed a sensitivity analysis to evaluate which absolute LNH threshold may better differentiate in volume the helical flow structures present in healthy controls and BAV patients. Our analysis led to a lower absolute LNH threshold of 0.6 which captured more volume elements to compare between groups allowing a more robust assessment. Furthermore, intra-observer segmentation error was similar previous studies, our study 5% vs. 6% in reference (47). In the same study of van Ooij et al. a scan retest assessment was performed and a segmentation error of 6% was reported between scans. In our study any subject was rescanned. Absolute LNH showed an intra-observer absolute error of 7% which is similar to other 4D flow velocity derived measurements such as wall shear stress (8% of error) (47) or energy loss (15% of error) (48).

Helical flow in BAV and aortic dilatation

Previous studies have associated BAV with eccentric flow and elevated flow helicity in the mid-ascending aorta section, and suggested that these flow alterations may contribute to the dilatation of the aorta (13,26,28,29,49,50). In this study, absolute LNH in the ascending aorta was significantly elevated in BAV patients as compared with healthy controls. Lorenz et al. reported a similar significant (P<0.001) difference between controls and BAV with

aortic dilatation along the thoracic aorta and the cardiac cycle for absolute LNH using 2D analysis planes. However, the 2D analysis strategy can underestimate reported absolute LNH (values <0.6) in the same way that peak velocity may be underestimated using 2D analysis plane strategy by sub-sampling the 3D velocity field (51,52). The absolute LNH MIPs used in our study (Fig. 2) allowed for the observation that absolute LNH >0.6 can be measured in heathy controls and its intensity increased in BAV patients. These results aligned with those reported by Morbiducci et al. (13,24). Furthermore, this study demonstrated that absolute LNH was associated with maximal aortic diameter of the ascending aorta. This hypothesis was suggested in previous studies where the qualitative grade of helicity was associated with mid-ascending aorta diameter (5,29,50). It is important to note that the association of absolute LNH with maximal aortic diameter was higher than the peak velocity (R=0.83 vs. R=0.46), and aortic valve effective orifice area (R=0.83 vs. R=−0.31). Furthermore, after adjusting aortic diameter by age, the correlations remained similar for both controls and BAV (Table 3). Thus, age may have a minimal influence in the association of aortic diameter with absolute LNH. Absolute LNH may potentially provide further detail of altered flow hemodynamics, beyond that of the aortic diameter growth rate, and elicit insight into fluid-wall interactions that may cause atherogenesis and/or atherosclerosis (10).

Impact of valve diseases

It has been demonstrated that BAV with aortic stenosis produce a significant (P<0.001) change in absolute LNH (26) as compared with heathy controls. The approach used in this study confirmed that absolute LNH has a significant association with the maximal ascending aorta diameter. Note that peak velocity rather than valve effective orifice area demonstrated a greater association with absolute LNH (Fig. 5). The elevated absolute LNH during the diastolic phase may be due to aortic valve insufficiency, the inertial effects of the diastolic flow, aortic compliance and pulse-wave reflection (4). Furthermore, systole deceleration and diastolic helicity may play a role in the aortic valve closing mechanism by avoiding turbulence and the left ventricle overload (53–56).

Relation between helical flow and shear forces

Shear forces may occur over the entire flow domain and not just at the aortic wall. It has been demonstrated that various components of the shear tensor, in particular shear gradients, directly influences platelet aggregation (57). In addition, helical flow and vortex shedding may also play an important role in the platelet deposition at physiological Reynolds number (22,58,59). Recently, Tovar-Lopez et al. demonstrated that the initiation of platelet aggregation is due to the shear gradient mechanism and the vortex formation constitute a secondary process that may serve to accelerate platelet aggregation process once the initial platelet mass has been established (60). Otherwise, elevated wall shear stress may be marginally related to platelet aggregation and activation. However, it may be a factor in the dysregulation of the extracellular matrix and elastic fiber degeneration in the ascending aorta of BAV patients (9). In particular, wall shear stress directionality has been shown to be related to the helical flow topology within the thoracic aorta (25). Furthermore, some studies have suggested that the helicity quantification in combination with wall shear stress (WSS) may be a valuable strategy for the prediction of dilatation rate, aneurysm formation and rupture (6,14,25,28). In this study, a method to quantify flow helicity was proposed. Helicity

quantification may thus be an important tool to better characterize both platelet aggregation and tissue degeneration in the thoracic aorta.

Study Limitations

This study included 50 BAV patients with a broad range of velocities, mid-ascending aorta diameters, and aortic insufficiency. The association between BAV phenotypes and absolute LNH was not explored in this study. The role of aortic insufficiency in the increment of absolute LNH was not possible due to the small number of severe cases (n=10) included in the BAV group. Patients follow-up was not available to assess the association of absolute LNH with aorta diameter grow rate, which might be helpful to demonstrate that aortic diameter enlargement can be predicted by absolute LNH. The main limitation of the LNH calculation is its dependence on spatial resolution, sensitivity to the velocity encoding selection (26), and data pre-processing (31). It should be notice that absolute LNH calculation was completely automated to reduce potential propagation error or post-processing settings. The LNH accuracy, error propagation and uncertainties mainly depend on the choice of differentiation scheme used (38,39). Any calculation involving partial derivatives from the velocity field will be affected by the spatial resolution. In particular, for helical flow and vortex detection the error transmission ratio is a function of Δ/L, where Δ corresponds to the spatial resolution and L to the length scale of the vortex (39). Thus, coarse sampling equals the Nyquist frequency ($\Delta/L=0.5$), i.e. for our subjects groups only helical flow with vortex cores >7.4 mm are properly mapped. For this study, a fourth-order scheme compact Richardson was used due its stability in a broad range of velocities, spatial resolutions, and signal-to-noise ratio (38,39). The effect of velocity encoding selection, without aliasing, will produce similar median values of helicity but the variance will be reduced with higher velocity encoding selection (26). Aliasing will lead to incorrect helicity values but its effect can be reduced using appropriate unwrapping algorithms. Furthermore, helicity calculation involves higher-order spatial derivatives which may naturally reflect the scale-wise energy dissipation (21). At the macro scale, cascade of eddies, helicity may be expected to dissipate faster than the kinetic energy. While at smaller scales (Kolmogorov scale on the order of mm to microns) only the kinetic energy dissipation plays a major role. For apparent turbulence in blood flow the scale is on the orders of tens of microns (61). Thus, 4D flow MRI derived parameters characterize the upper portion of energy dissipation process at small scale. A more formal analysis of energy dissipation using 4D flow MRI data may be explored by means of dynamic mode decomposition and/or modal mode decomposition. These methods are closely related with scale-spatial flow energy dissipation and have shown the potential to characterize complex fluids in cardiovascular models (62). Otherwise, flow turbulence can better be characterized with 4D flow MRI using the quantification of turbulent kinetic energy (63,64). Furthermore, in this study the aortic vessel geometry/shape was not assessed. A recent study of Frydrychowicz et al.(14) evaluated this geometrical/shape aspect and found that vortex formation was prominent in the ascending aorta (50.0%), followed by the descending aorta (40.2%) and the arch (9.8%). In addition, it was a significant association between arch geometry and the presence of helicity (P=0.001). In our study LNH presented a similar pattern (Fig. 4) with increased LNH in the ascending aorta, followed by the descending aorta and then the aortic arch.

CONCLUSION

In conclusion, this study demonstrated that absolute LNH can differentiate helical flow alterations between healthy controls and BAV patients using an optimal threshold. Absolute LNH was associated with maximal aorta diameter of the ascending aorta. LNH was associated with aortic stenosis severity, however no significant differences between aortic stenosis grading groups were found.

Supplementary Material

Refer to Web version on PubMed Central for supplementary material.

Acknowledgements

This work was supported by National Institute of Health (NIH) National Heart, Lung, and Blood Institute (NHLBI) grant R01HL115828, K25HL119608, and American Heart Association (AHA) 14POST18350019.

References

1. Alastruey J, Siggers JH, Peiffer V, Doorly DJ, Sherwin SJ. Reducing the data: Analysis of the role of vascular geometry on blood flow patterns in curved vessels. Phys. Fluids. 2012:24.
2. Bogren HG, Buonocore MH. 4D magnetic resonance velocity mapping of blood flow patterns in the aorta in young vs. elderly normal subjects. J. Magn. Reson. Imaging. 1999; 10:861–9. [PubMed: 10548800]
3. Buonocore MH, Bogren HG. Analysis of flow patterns using MRI. Int. J. Card. Imaging. 1999; 15:99–103. [PubMed: 10453408]
4. Kilner PJ, Yang GZ, Mohiaddin RH, Firmin DN, Longmore DB. Helical and retrograde secondary flow patterns in the aortic arch studied by three-directional magnetic resonance velocity mapping. Circulation. 1993; 88:2235–2247. [PubMed: 8222118]
5. Bissell MM, Hess AT, Biasiolli L, et al. Aortic dilation in bicuspid aortic valve disease: flow pattern is a major contributor and differs with valve fusion type. Circ. Cardiovasc. Imaging. 2013; 6:499–507. [PubMed: 23771987]
6. Mahadevia R, Barker AJ, Schnell S, et al. Bicuspid Aortic Cusp Fusion Morphology Alters Aortic 3D Outflow Patterns, Wall Shear Stress and Expression of Aortopathy. Circulation. 2013:673–682.
7. Hope TA, Markl M, Wigström L, Alley MT, Miller DC, Herfkens RJ. Comparison of flow patterns in ascending aortic aneurysms and volunteers using four-dimensional magnetic resonance velocity mapping. J. Magn. Reson. Imaging. 2007; 26:1471–9. [PubMed: 17968892]
8. Barker AJ, Markl M, Bürk J, Lorenz R, Bock J, Bauer S, Schulz-Menger J, von Knobelsdorff-Brenkenhoff F. Bicuspid aortic valve is associated with altered wall shear stress in the ascending aorta. Circ. Cardiovasc. Imaging. 2012; 5:457–66. [PubMed: 22730420]
9. Guzzardi DG, Barker AJ, van Ooij P, et al. Valve-Related Hemodynamics Mediate Human Bicuspid Aortopathy. J. Am. Coll. Cardiol. 2015; 66:892–900. [PubMed: 26293758]
10. Malek AM, Alper SL, Izumo S. Hemodynamic shear stress and its role in atherosclerosis. JAMA. 1999; 282:2035–42. [PubMed: 10591386]
11. Fedak PWM, Verma S, David TE, Leask RL, Weisel RD, Butany J. Clinical and Pathophysiological Implications of a Bicuspid Aortic Valve. Circulation. 2002; 106:900–904. [PubMed: 12186790]
12. Markl M, Harloff A, Bley TA, Zaitsev M, Jung B, Weigang E, Langer M, Hennig J, Frydrychowicz A. Time-resolved 3D MR velocity mapping at 3T: improved navigator-gated assessment of vascular anatomy and blood flow. J. Magn. Reson. Imaging. 2007; 25:824–31. [PubMed: 17345635]
13. Morbiducci U, Ponzini R, Rizzo G, Cadioli M, Esposito A, De Cobelli F, Del Maschio A, Montevecchi FM, Redaelli A. In vivo quantification of helical blood flow in human aorta by time-

resolved three-dimensional cine phase contrast magnetic resonance imaging. Ann. Biomed. Eng. 2009; 37:516–31. [PubMed: 19142728]

14. Frydrychowicz A, Berger A, Munoz Del Rio A, Russe MF, Bock J, Harloff A, Markl M. Interdependencies of aortic arch secondary flow patterns, geometry, and age analysed by 4-dimensional phase contrast magnetic resonance imaging at 3 Tesla. Eur. Radiol. 2012; 22:1122–30. [PubMed: 22207269]
15. Clough RE, Waltham M, Giese D, Taylor PR, Schaeffter T. A new imaging method for assessment of aortic dissection using four-dimensional phase contrast magnetic resonance imaging. J. Vasc. Surg. 2012; 55:914–23. [PubMed: 22386146]
16. Frydrychowicz A, Markl M, Hirtler D, Harloff A, Schlensak C, Geiger J, Stiller B, Arnold R. Aortic hemodynamics in patients with and without repair of aortic coarctation: in vivo analysis by 4D flow-sensitive magnetic resonance imaging. Invest. Radiol. 2011; 46:317–325. [PubMed: 21285892]
17. Frydrychowicz A, Harloff A, Jung B, Zaitsev M, Weigang E, Bley TA, Langer M, Hennig J, Markl M. Time-resolved, 3-dimensional magnetic resonance flow analysis at 3 T: visualization of normal and pathological aortic vascular hemodynamics. J. Comput. Assist. Tomogr. 2007; 31:9–15. [PubMed: 17259827]
18. Garcia J, Capoulade R, Le Ven F, Gaillard E, Kadem L, Pibarot P, Larose É. Discrepancies between cardiovascular magnetic resonance and Doppler echocardiography in the measurement of transvalvular gradient in aortic stenosis: the effect of flow vorticity. J. Cardiovasc. Magn. Reson. 2013; 15:84. [PubMed: 24053194]
19. Hunt JCR, Hussain F, Physics T, Street S. A note on velocity, vorticity and helicity of inviscid fluid elements. J. Fluid Mech. 1991; 229:569–587.
20. Köhler B, Gasteiger R, Preim U, et al. Semi-automatic vortex extraction in 4D PC-MRI cardiac blood flow data using line predicates. IEEE Trans. Vis. Comput. Graph. 2013; 19:2773–82. [PubMed: 24051844]
21. Moffatt HK, Tsinober A. Helicity in Laminar and Turbulent Flow. Annu. Rev. Fluid Mech. 1992; 24:281–312.
22. Liu X, Sun A, Fan Y, Deng X. Physiological Significance of Helical Flow in the Arterial System and its Potential Clinical Applications. Ann. Biomed. Eng. 2014; 43:3–15. [PubMed: 25169424]
23. Morbiducci U, Ponzini R, Gallo D, Bignardi C, Rizzo G. Inflow boundary conditions for image-based computational hemodynamics: Impact of idealized versus measured velocity profiles in the human aorta. J. Biomech. 2013; 46:102–109. [PubMed: 23159094]
24. Morbiducci U, Ponzini R, Rizzo G, Cadioli M, Esposito A, Montevecchi FM, Redaelli A. Mechanistic insight into the physiological relevance of helical blood flow in the human aorta: an in vivo study. Biomech. Model. Mechanobiol. 2011; 10:339–55. [PubMed: 20652615]
25. Morbiducci U, Gallo D, Cristofanelli S, Ponzini R, Deriu MA, Rizzo G, Steinman DA. A rational approach to defining principal axes of multidirectional wall shear stress in realistic vascular geometries, with application to the study of the influence of helical flow on wall shear stress directionality in aorta. J. Biomech. 2015; 48:899–906. [PubMed: 25748224]
26. Lorenz R, Bock J, Barker AJ, et al. 4D flow magnetic resonance imaging in bicuspid aortic valve disease demonstrates altered distribution of aortic blood flow helicity. Magn. Reson. Med. 2014; 71:1542–53. [PubMed: 23716466]
27. Gallo D, Steinman DA, Bijari PB, Morbiducci U. Helical flow in carotid bifurcation as surrogate marker of exposure to disturbed shear. J. Biomech. 2012; 45:2398–404. [PubMed: 22854207]
28. Hope MD, Hope TA, Crook SE, Ordovas KG, Urbania TH, Alley MT, Higgins CB. 4D flow CMR in assessment of valve-related ascending aortic disease. JACC. Cardiovasc. Imaging. 2011; 4:781–7. [PubMed: 21757170]
29. Hope MD, Hope TA, Meadows AK, Ordovas KG, Urbania TH, Alley MT, Higgins CB. Bicuspid aortic valve: four-dimensional MR evaluation of ascending aortic systolic flow patterns. Radiology. 2010; 255:53–61. [PubMed: 20308444]
30. Cawley PJ, Maki JH, Otto CM. Cardiovascular magnetic resonance imaging for valvular heart disease: technique and validation. Circulation. 2009; 119:468–78. [PubMed: 19171869]

31. Bock J, Kreher BW, Hennin J, Markl M. Optimized pre-processing of time-resolved 2D and 3D phase contrast MRI data. 15th Scientific Meeting International Society for Magnetic Resonance in Medicine. 2007:3138.
32. Garcia J, Barker AJ, van Ooij P, Schnell S, Puthumana J, Bonow RO, Collins JD, Carr JC, Markl M. Assessment of altered three-dimensional blood characteristics in aortic disease by velocity distribution analysis. Magn. Reson. Med. 2015; 74:817–825. [PubMed: 25252029]
33. Garcia J, Jarvis KB, Schnell S, Malaisrie SC, Clennon C, Collins JD, Carr JC, Markl M, Barker AJ. 4D flow MRI of the aorta demonstrates age- and gender-related differences in aortic size and blood flow velocity in healthy subjects. J. Cardiovasc. Magn. Reson. 2015; 17:P39.
34. Garcia J, Barker AJ, Murphy I, Jarvis K, Schnell S, Collins JD, Carr JC, Malaisrie SC, Markl M. Four-dimensional flow magnetic resonance imaging-based characterization of aortic morphometry and haemodynamics: impact of age, aortic diameter, and valve morphology. Eur. Hear. J. – Cardiovasc. Imaging. 2015:jev228. doi: 10.1093/ehjci/jev228.
35. Nishimura RA, Otto CM, Bonow RO, et al. 2014 AHA/ACC Guideline for the Management of Patients With Valvular Heart Disease: Executive Summary: A Report of the American College of Cardiology/American Heart Association Task Force on Practice Guidelines. Circulation. 2014; 129:2440–2492. [PubMed: 24589852]
36. Garcia J, Marrufo OR, Rodriguez AO, Larose E, Pibarot P, Kadem L. Cardiovascular magnetic resonance evaluation of aortic stenosis severity using single plane measurement of effective orifice area. J. Cardiovasc. Magn. Reson. 2012; 14:23. [PubMed: 22480269]
37. Garcia J, Markl M, Schnell S, Allen B, Entezari P, Mahadevia R, Chris Malaisrie S, Pibarot P, Carr J, Barker AJ. Evaluation of aortic stenosis severity using 4D flow jet shear layer detection for the measurement of valve effective orifice area. Magn. Reson. Imaging. 2014; 32:891–898. [PubMed: 24865143]
38. Garcia J, Larose E, Pibarot P, Kadem L. On the evaluation of vorticity using cardiovascular magnetic resonance velocity measurements. J. Biomech. Eng. 2013; 135:124501–6. [PubMed: 24026138]
39. Etebari A, Vlachos PP. Improvements on the accuracy of derivative estimation from DPIV velocity measurements. Exp. Fluids. 2005; 39:1040–1050.
40. Hiratzka LF, Bakris GL, Beckman JA, et al. 2010 ACCF/AHA/AATS/ACR/ASA/SCA/SCAI/SIR/STS/SVM Guidelines for the diagnosis and management of patients with thoracic aortic disease. A Report of the American College of Cardiology Foundation/American Heart Association Task Force on Practice Guidelines, A. J. Am. Coll. Cardiol. 2010; 55:e27–e129. [PubMed: 20359588]
41. Michelena HI, Prakash SK, Della Corte A, et al. Bicuspid Aortic Valve: Identifying Knowledge Gaps and Rising to the Challenge From the International Bicuspid Aortic Valve Consortium (BAVCon). Circulation. 2014; 129:2691–704. [PubMed: 24958752]
42. Forte A, Della Corte A, Grossi M, et al. Early cell changes and TGFβ pathway alterations in the aortopathy associated with bicuspid aortic valve stenosis. Clin. Sci. 2012; 124:97–108.
43. Moffatt HK. Helicity and singular structures in fluid dynamics. Proc. Natl. Acad. Sci. 2014; 111:3663–3670. [PubMed: 24520175]
44. Caro CG, Doorly DJ, Tarnawski M, Scott KT, Long Q, Dumoulin CL. Non-Planar Curvature and Branching of Arteries and Non-Planar-Type Flow. Proc. R. Soc. A Math. Phys. Eng. Sci. 1996; 452:185–197.
45. Stonebridge PA, Hoskins PR, Allan PL, Belch JF. Spiral laminar flow in vivo. Clin. Sci. (Lond). 1996; 91:17–21. [PubMed: 8774255]
46. Strecker C, Harloff A, Wallis W, Markl M. Flow-sensitive 4D MRI of the thoracic aorta: comparison of image quality, quantitative flow, and wall parameters at 1.5 T and 3 T. J. Magn. Reson. Imaging. 2012; 36:1097–103. [PubMed: 22745007]
47. van Ooij P, Powell AL, Potters WV, Carr JC, Markl M, Barker AJ. Reproducibility and interobserver variability of systolic blood flow velocity and 3D wall shear stress derived from 4D flow MRI in the healthy aorta. J. Magn. Reson. Imaging. 2016; 43:236–48. [PubMed: 26140480]
48. van Ooij P, Allen BD, Contaldi C, Garcia J, Collins J, Carr J, Choudhury L, Bonow RO, Barker AJ, Markl M. 4D flow MRI and T 1 -Mapping: Assessment of altered cardiac hemodynamics and

extracellular volume fraction in hypertrophic cardiomyopathy. J. Magn. Reson. Imaging. 2016; 43:107–114. [PubMed: 26227419]

49. Faggiano E, Antiga L, Puppini G, Quarteroni A, Luciani GB, Vergara C. Helical flows and asymmetry of blood jet in dilated ascending aorta with normally functioning bicuspid valve. Biomech. Model. Mechanobiol. 2012
50. Bürk J, Blanke P, Stankovic Z, Barker A, Russe M, Geiger J, Frydrychowicz A, Langer M, Markl M. Evaluation of 3D blood flow patterns and wall shear stress in the normal and dilated thoracic aorta using flow-sensitive 4D CMR. J. Cardiovasc. Magn. Reson. 2012; 14:84. [PubMed: 23237187]
51. Bieging ET, Frydrychowicz A, Wentland A, Landgraf BR, Johnson KM, Wieben O, François CJ. In vivo three-dimensional MR wall shear stress estimation in ascending aortic dilatation. J. Magn. Reson. Imaging. 2011; 33:589–597. [PubMed: 21563242]
52. Garcia J, Capoulade R, Le Ven F, Gaillard E, Kadem L, Pibarot P, Larose É. Discrepancies between cardiovascular magnetic resonance and Doppler echocardiography in the measurement of transvalvular gradient in aortic stenosis: the effect of flow vorticity. J. Cardiovasc. Magn. Reson. 2013; 15:84. [PubMed: 24053194]
53. Macagno, E. Leonardian fluid mechanics. IIHR Monographs; Iowa: 1988.
54. Nasiraei Moghaddam A, Saber NR, Wen H, et al. Analytical method to measure three-dimensional strain patterns in the left ventricle from single slice displacement data. J. Cardiovasc. Magn. Reson. 2010; 12:33. [PubMed: 20515489]
55. Gharib M, Kremers D, Koochesfahani MM, Kemp M. Leonardo's vision of flow visualization. Exp. Fluids. 2002; 33:219–223.
56. Garcia J, Pibarot P, Capoulade R, Le Ven F, Kadem L, Larose E, Larose É. Usefulness of cardiovascular magnetic resonance imaging for the evaluation of valve opening and closing kinetics in aortic stenosis. Eur. Heart J. Cardiovasc. Imaging. 2013; 14:819–826. [PubMed: 23299400]
57. Nesbitt WS, Westein E, Tovar-Lopez FJ, Tolouei E, Mitchell A, Fu J, Carberry J, Fouras A, Jackson SP. A shear gradient-dependent platelet aggregation mechanism drives thrombus formation. Nat. Med. 2009; 15:665–73. [PubMed: 19465929]
58. Bluestein D, Gutierrez C, Londono M, Schoephoerster RT, Luestein DAB, Utierrez CAG, Ondono MAL. Vortex shedding in steady flow through a model of an arterial stenosis and its relevance to mural platelet deposition. Ann. Biomed. Eng. 1999; 27:763–73. [PubMed: 10625149]
59. Shadden SC, Hendabadi S. Potential fluid mechanic pathways of platelet activation. Biomech. Model. Mechanobiol. 2013; 12:467–474. [PubMed: 22782543]
60. Tovar-Lopez FJ, Rosengarten G, Nasabi M, Sivan V, Khoshmanesh K, Jackson SP, Mitchell A, Nesbitt WS. An Investigation on Platelet Transport during Thrombus Formation at Micro-Scale Stenosis. PLoS One. 2013; 8:e74123. [PubMed: 24194822]
61. Antiga L, Steinman DA. Rethinking turbulence in blood. Biorheology. 2009; 46:77–81. [PubMed: 19458411]
62. Kefayati S, Poepping TL. Transitional flow analysis in the carotid artery bifurcation by proper orthogonal decomposition and particle image velocimetry. Med. Eng. Phys. 2012; 35:898–909. [PubMed: 23025907]
63. Dyverfeldt P, Kvitting J-PE, Sigfridsson A, et al. Assessment of fluctuating velocities in disturbed cardiovascular blood flow: in vivo feasibility of generalized phase-contrast MRI. J. Magn. Reson. Imaging. 2008; 28:655–63. [PubMed: 18777557]
64. Dyverfeldt P, Hope MD, Tseng EE, Saloner D. Magnetic resonance measurement of turbulent kinetic energy for the estimation of irreversible pressure loss in aortic stenosis. JACC. Cardiovasc. Imaging. 2013; 6:64–71. [PubMed: 23328563]

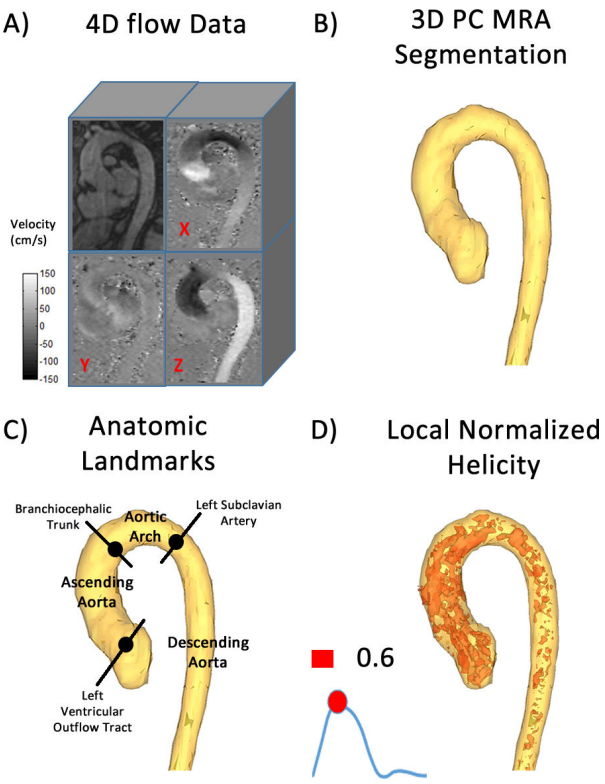

FIGURE 1. Workflow for the assessment of absolute local normalized helicity (LNH)

Workflow for the assessment of absolute local normalized helicity (LNH). 4D flow data (A) were used for calculating a phase contrast MR angiogram (MRA). The MRA was used to segment the entire aorta (B). Anatomic landmarks (C) identifying the location of the left ventricular outflow tract, the branchiocephalic trunk, and the left subclavian artery were used. Anatomic landmarks were used to divide the aorta into three sub-domains: 1) ascending aorta, 2) aortic arch, and 3) descending aorta. Absolute LNH was computed within the entire aorta segmentation (D). Absolute LNH 3D features were visualized and quantified using a threshold of 0.6.

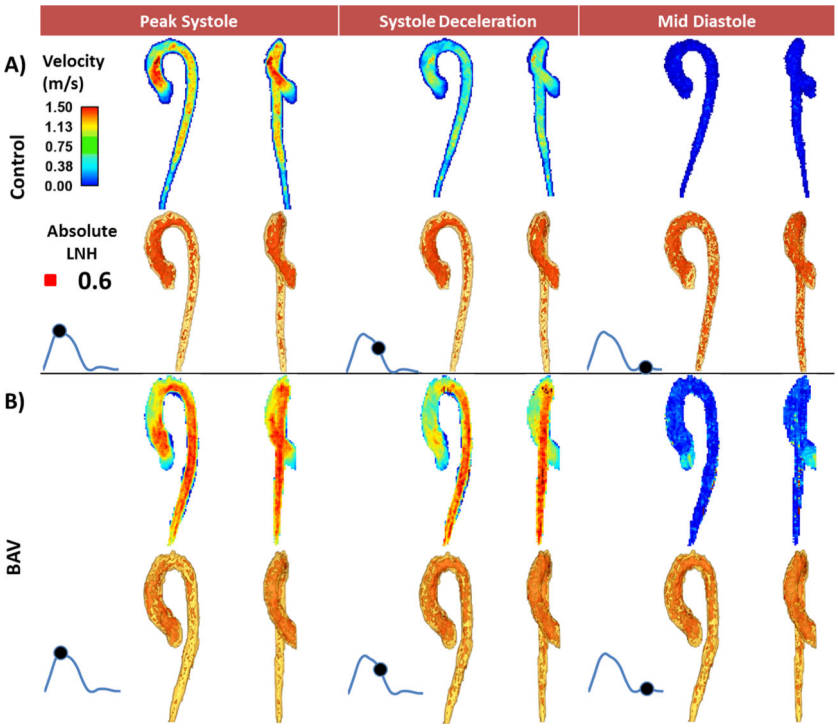

FIGURE 2. Comparison of absolute local normalized helicity in the entire aorta between one healthy control and one patient with bicuspid aortic valve (BAV)

Comparison of absolute local normalized helicity in the entire aorta between one healthy control and one patient with bicuspid aortic valve (BAV). The horizontal panels show a healthy control subject (mid-ascending aorta diameter = 27 mm) (A) and a patient (B) with BAV (mid-ascending aorta diameter = 28 mm). The first row illustrates the aortic flow velocity maximum intensity projection (MIP) and the second row shows absolute local normalized helicity (LNH) 3D features; the first column shows both velocity and absolute LNH MIPs at peak systole; the second column at systolic deceleration and the third column at mid-diastole.

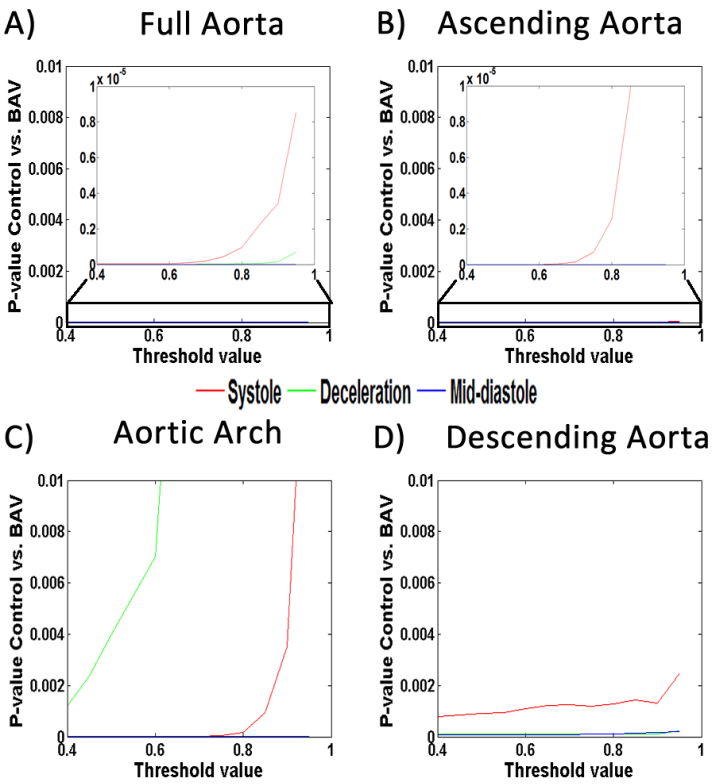

FIGURE 3. Absolute local normalized helicity sensitivity analysis

Absolute local normalized helicity sensitivity analysis. The analysis was perform in the full aorta (A), the ascending aorta (B), the aortic arch (C), and the descending aorta (D). Sub-plot in panel A and B corresponds to the zoomed area within the black rectangle. P-values <0.01 were obtained using a threshold of 0.6.

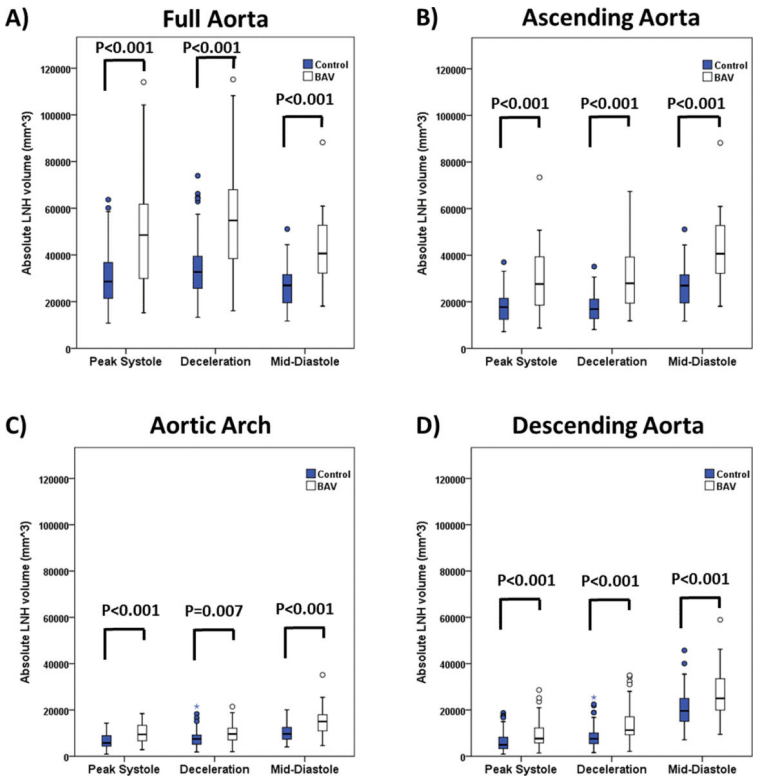

FIGURE 4. Absolute local normalized helicity comparison between healthy controls and patients for all segments

Absolute local normalized helicity comparison between healthy controls and patients for all segments. Volume corresponded to absolute local normalized helicity (LNH) >0.6. Analysis segments corresponded to the full aorta (A) which was further sub-divided on ascending aorta (B), aortic arch (C), and descending aorta (D). Comparison between healthy controls vs. BAV groups was given by a *t-test*. Outliers, circles, were defined by 1.5 × interquartile range. Extreme values, stars, were defined by 3 × interquartile range.

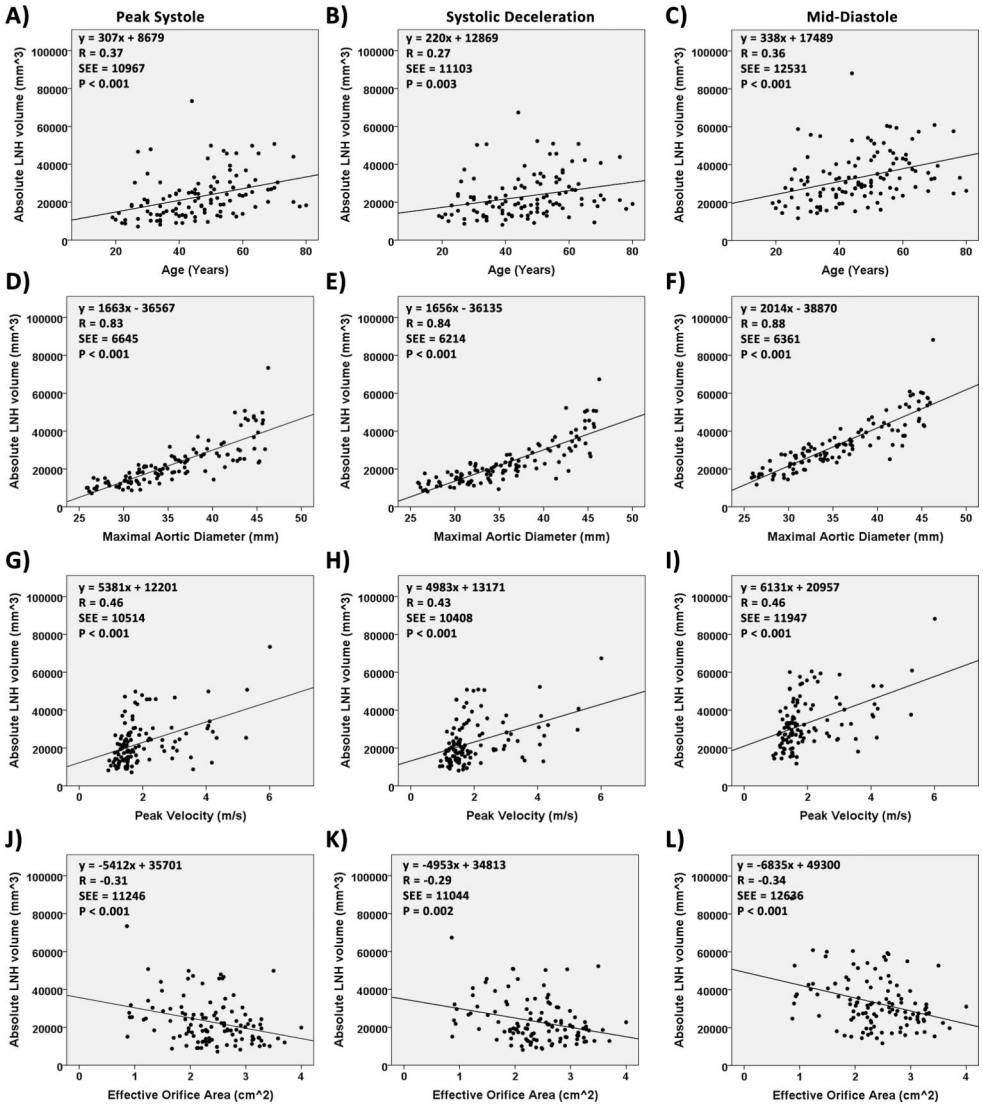

FIGURE 5. Regression plots for absolute local normalized helicity

Regression plots for absolute local normalized helicity. Volume corresponded to absolute local normalized helicity (LNH) >0.6. Panels A-C show the regression plots between absolute normalized helicity and age. Panels D-F show the regression plots between absolute normalized helicity and maximal aortic diameter. Panels G-I show the regression plots between absolute normalized helicity and peak velocity. Panels J-L show the regression plots between absolute normalized helicity and aortic valve effective orifice area.

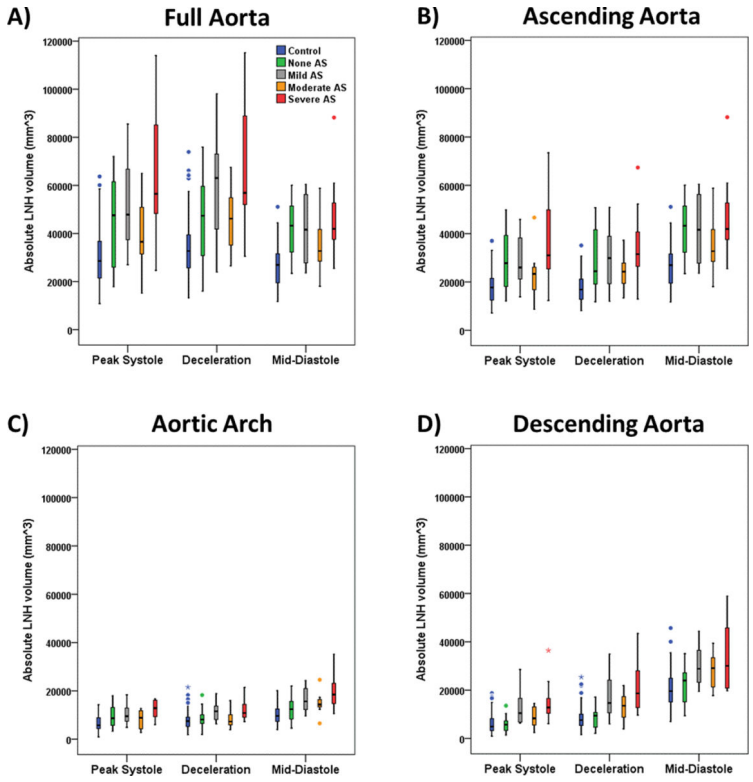

FIGURE 6. Comparison of absolute local normalized helicity between aortic stenosis severity groups and controls

Comparison of absolute local normalized helicity between aortic stenosis severity groups and controls. Volume corresponded to absolute local normalized helicity (LNH) >0.6. Analysis segments corresponded to the full aorta (A) which was further sub-divided on ascending aorta (B), aortic arch (C), and descending aorta (D). Comparison between healthy controls and BAV stenosis severity groups are summarized in Table 4. Outliers, circles, were defined by 1.5 × interquartile range. Extreme values, stars, were defined by 3 × interquartile range.

Table 1

Velocity encoding and spatial resolution

		Velocity Encoding (m/s)	Spatial Resolution (mm)
Control		150	1.66-2.81 × 1.66-2.81 × 2.20-2.85
Bicuspid Aortic Valve	None	150-250	2.12-2.50 × 2.50-2.73 × 2.40-3.50
	Mild	150-300	2.12-2.73 × 2.12-2.73 × 2.40-3.00
	Moderate	150-400	2.12-2.73 × 2.12-2.73 × 2.00-3.00
	Severe	150-400	2.12-2.73 × 2.12-2.73 × 2.60-3.50

Table 2

Patient Characteristics

	Controls	BAV	P-value Controls vs. BAV
N	65	50	
Age (years)	43±14 (78,19)	49±14 (80,23)	0.017
Female	25 (38%)	12 (24%)	0.101
Height (m)	1.72±0.08 (1.90,1.52)	1.77±0.08 (1.96,1.55)	0.002
Weight (kg)	84±19 (136,54)	83±13 (123,59)	-
Maximal aortic diameter (mm)	33±4 (26,41)	40±5 (28,46)	<0.001
Effective Orifice Area (cm^2)	2.6±0.5 (1.8,4.0)	2.0±0.7 (0.9,3.5)	<0.001
Stenosis Severity			
Mild	0 (0%)	12 (24%)	<0.001
Moderate	0 (0%)	7 (14%)	0.046
Severe	0 (0%)	10 (20%)	<0.001
Regurgitation Severity			
Mild	0 (0%)	6 (12%)	0.004
Moderate	0 (0%)	4 (8%)	0.021
Severe	0 (0%)	1 (2%)	-

All continuous data are presented as mean±standard deviation (max,min) or number (%). BAV indicates bicuspid aortic valve. P-value resulted from independent-sample *t*-test (Gaussian distribution) or Mann-Whitney (non-Gaussian distribution) comparing subjects groups.

Table 3

Associations with absolute local normalized helicity

Maximal aortic diameter	Absolute LNH at peak systole		Absolute LNH at systolic deceleration		Absolute LNH at mid-diastole	
	R	P-value	R	P-value	R	P-value
Controls	0.84	<0.001	0.74	<0.001	0.84	<0.001
Bicuspid aortic valve	0.75	<0.001	0.80	<0.001	0.81	<0.001
Age adjusted maximal aortic diameter						
Control	0.84	<0.001	0.75	<0.001	0.84	<0.001
Bicuspid aortic valve	0.75	<0.001	0.80	<0.001	0.81	<0.001

Table 4

Comparison of absolute local normalized helicity between aortic stenosis severity groups and controls

		Absolute LNH at peak systole	Absolute LNH at systolic deceleration	Absolute LNH at mid-diastole
Full Aorta	Control vs. None AS	**0.005**	**0.004**	**<0.001**
	Control vs. Mild AS	**<0.001**	**<0.001**	**<0.001**
	Control vs. Moderate AS	0.1	**0.047**	**0.05**
	Control vs. Severe AS	**<0.001**	**<0.001**	**<0.001**
Ascending Aorta	Control vs. None AS	**<0.001**	**<0.001**	**<0.001**
	Control vs. Mild AS	**<0.001**	**<0.001**	**<0.001**
	Control vs. Moderate AS	0.174	**0.022**	**0.05**
	Control vs. Severe AS	**<0.001**	**<0.001**	**<0.001**
Aortic Arch	Control vs. None AS	**<0.001**	0.312	**0.030**
	Control vs. Mild AS	**0.002**	**0.004**	**<0.001**
	Control vs. Moderate AS	0.43	0.669	**0.016**
	Control vs. Severe AS	**<0.001**	**0.003**	**<0.001**
Descending Aorta	Control vs. None AS	0.908	0.790	0.322
	Control vs. Mild AS	**0.001**	**<0.001**	**<0.001**
	Control vs. Moderate AS	0.141	**0.045**	**0.028**
	Control vs. Severe AS	**<0.001**	**<0.001**	**<0.001**

Comparison between healthy controls vs. BAV stenosis severity groups was given by a Mann-Whitney test. P-values ≤ 0.05 are bold.